Highly coherent room-temperature molecular polariton condensates

Daegwang Choi, Serena Zachariah, Ravindra Kumar Yadav, and Vinod. M. Menon**

Daegwang Choi, Serena Zachariah, Ravindra Kumar Yadav, Vinod. M. Menon
Department of Physics, The City College of New York, 85 St. Nicholas Terrace, New York, New York 10031, United States
E-mail: vmenon@ccny.cuny.edu, dchoi@ccny.cuny.edu

Ravindra Kumar Yadav
School of Physical Sciences, Indian Institute of Technology Mandi, Mandi 175005, Himachal Pradesh, India

Keywords: organic dye, exciton-polariton, polariton lasing, light-matter interaction, microcavity

Abstract

A growing number of organic materials have recently been reported to achieve room-temperature exciton-polariton (polariton) condensation, which is an essential requirement for practical polaritonic applications. Notably, fluorescent dyes utilizing the small-molecule, ionic isolation lattice (SMILES) method have solved the long-standing challenges of conventional organic dyes and have been successfully implemented in cavities to realize condensation. However, almost all demonstrations of molecular polariton condensates have inherently large spectral linewidth and poor temporal coherence arising from intrinsic disorder and low quality (Q) factor of the cavity. Here, we realize exciton-polaritons using fluorescent dye SMILES in a high Q factor microcavity and observe polariton condensates with a linewidth of 175 μeV. These polariton condensates exhibit temporal coherence of 30.3 ± 8.0 ps, indicating the highly coherent nature of the narrow linewidth condensates. These results set the stage for realizing highly coherent and robust polaritonic devices operating at room temperature.

1. Introduction

Coherent light sources, such as lasers, have become fundamental to modern technology through their ability to produce highly directional, monochromatic light with coherence. While conventional photonic lasers are formed through a stimulated emission process and population

inversion, a polariton laser is realized by the polariton condensation, a coherent ground state with polaritons that result from the strong light-matter interactions.[1] Polariton lasers offer lower threshold power compared to the photonic laser, enabling the realization of energy-efficient coherent light sources.[2,3] Since the first observation of polariton condensation at cryogenic temperatures in 2006[1], the research for realizing room-temperature polariton condensates has flourished utilizing a wide range of novel materials.[4–6]

Organic materials, in particular, offer several distinct advantages for polariton devices due to their large exciton binding energy which arises from their Frenkel nature, synthetic tunability, room-temperature operation, flexibility, solution processability, and cost-effectiveness.[7,8] With all of these advantages, polariton condensation has been reported using various organic materials.[9–14] Furthermore, organic material-based polaritons have been utilized in a variety of applications such as optical switches[15], logic gates[16], transistors[17], analog Hamiltonian simulators[18,19], and Light-emitting diodes[20] at room temperature. In this context, there is great potential to realize room-temperature polariton devices with a broad range of wavelengths and optical properties using the countless fluorescent organic materials in nature. However, this remains challenging due to long-standing problems associated with fluorescent dyes such as aggregation, luminescence quenching, and structural instability.[21]

To overcome these fundamental limitations, the recent discovery of small-molecule ionic isolation lattices (SMILES) represents a breakthrough by spatially isolating dye molecules within a structured lattice and maintaining optimal dye-dye distance. SMILES are synthesized by mixing a commonly used fluorescent organic dye with a colorless anion-binding macrocycle called cyanostar, preventing dye aggregation, concentration quenching and significantly enhancing the photoluminescence (PL) quantum yield.[21]

Recently, SMILES has been effectively used to realize bright polariton condensates through Tamm plasmon (TP) polaritons in metal–distributed Bragg reflector (DBR) microcavity.[22] TPs can create highly confined electromagnetic states at the metal/DBR interface, leading to strong light–matter interactions. However, TP modes in metal/DBR cavities exhibit a relatively low Q factor, presenting a fundamental drawback for more practical polariton-based applications. Therefore, employing all-DBR-based microcavities is the optimal approach, yet direct deposition of top DBR can cause damage to the active material occasionally.[23] As an alternative approach involving transferring of pre-fabricated DBRs onto active materials has been reported as a method to avoid damage and achieve high Q factor cavities.[23–26]

Here, we demonstrate the strong coupling of fluorescent dye SMILES in DBR-based microcavities by employing pick-and-place DBR transfer technique, obtaining Rabi splitting

value of approximately 110 meV from reflectance measurements. By exciting the microcavity with a non-resonant pulsed laser, we observe room-temperature polariton condensation above the critical pumping power with ultra-narrow linewidth of 175 μeV. Furthermore, we demonstrate the emergence of spatial coherence above the threshold using a Michelson interferometer. Temporal coherence measurements reveal the coherence time of 30.3 ± 8.0 ps for the polariton condensates, which is an order of magnitude higher than previously reported values for planar microcavities.[11,27,28]

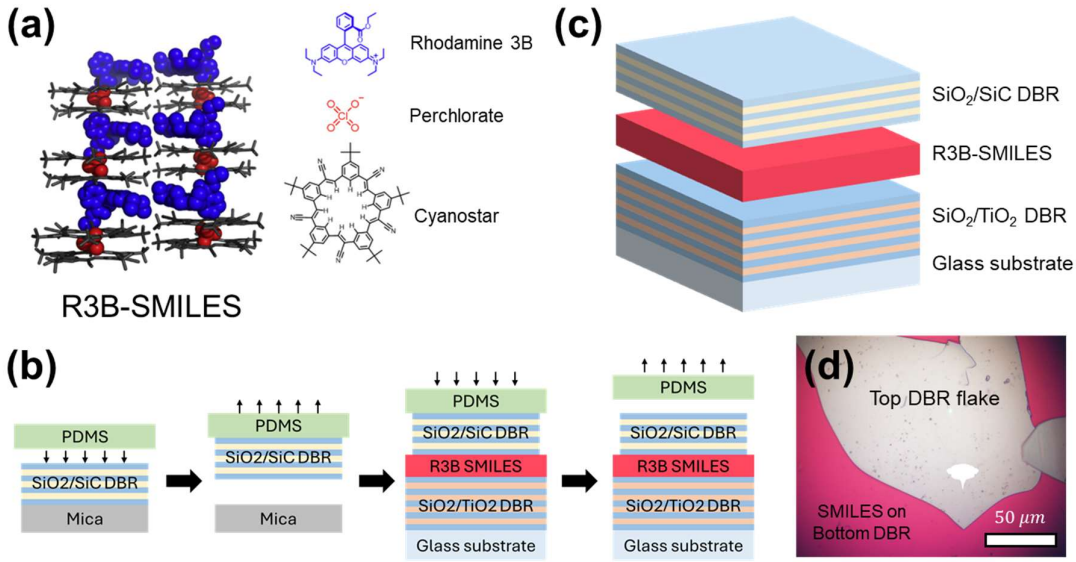

Figure 1. Schematic of organic microcavity and fabrication process. a) Chemical structure of Rhodamine 3B-SMILES and its ingredients: Rhodamine 3B, Perchlorate, and Cyanostar. b) Fabrication process of microcavity by top DBR transfer method. DBRs are deposited on mica and glass substrate for top and bottom DBR, respectively. DBR on mica is picked up and transferred to the R3B-SMILES coated bottom DBR with PDMS stamp. c) Simple illustration of organic-based planar microcavity structure. A sandwich structure of R3B-SMILES between two dielectric DBRs on a glass substrate d) Optical microscopic image of a transferred top DBR flake on the R3B-SMILES.

2. Experimental results

2.1. Sample fabrications

First, we synthesize the SMILES complex by using Rhodamine 3B (R3B) dye, a fluorescent dye that is commonly used as a gain medium for dye lasers. We combine R3B perchlorate (ClO4-) and cyanostar macrocycle in a chlorobenzene solvent. The SMILES solution is mixed with a polymethyl methacrylate (PMMA) solution, which helps control the thickness of SMILES thin film during the spin-coating process. The detailed synthesis method of SMILES

is described in Methods and reference.[22] When R3B dye forms a thin film, its quantum yield and fluorescence brightness are significantly reduced compared to its performance in solution, mainly due to molecular aggregation and exciton quenching in the solid state. However, R3B-SMILES overcomes these challenges by isolating the dye molecules within a molecular lattice. As a result, even in the crystallized thin film state, R3B-SMILES exhibits uniform and extremely bright fluorescence, improving brightness by approximately ten times compared to the original R3B dye thin films. The PL and absorption spectra of R3B-SMILES are provided in Reference.[22]

We deposit an R3B-SMILES thin film on the bottom DBR substrate by spin-coating the R3B-SMILES solution. The thickness of the R3B-SMILES thin film is approximately 200 nm, designed to create a cavity mode around a wavelength of 600 nm. To fabricate the top DBR structure, we fabricate SiC/SiO_2 DBR on a mica substrate using plasma-enhanced chemical vapor deposition. Due to the significant strain between the mica substrate and the DBR structure, the DBR easily delaminates from the mica substrate.[23] Figure 1b illustrates the step-by-step process of DBR transfer. We use polydimethylsiloxane (PDMS) to pick up the DBR and transfer it onto the prepared SMILES/DBR structures to make microcavities. Figure 1c shows simple illustrations of the fabricated microcavities. The deposited DBR is already fragmented on the mica substrate, and when lifted with the PDMS, all portions of the DBR in contact with the PDMS delaminate from the mica. However, not all the DBR fragments transfer onto the SMILES layer, resulting in a random distribution of DBR flakes. Figure 1d shows an optical microscopic image of a DBR flake on the SMILES/DBR structure. A typical DBR flake size is the order of 100 μm.

2.2. Angle-resolved reflectance spectroscopy

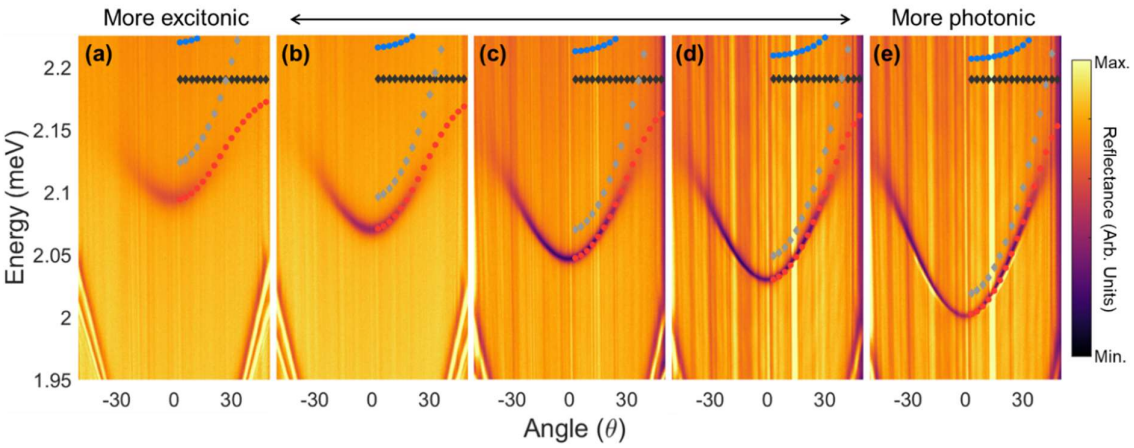

Figure 2. Energy-momentum dispersion of polaritons. a-e) Angle-resolved reflectance spectra of lower polaritons depending on the detuning. From a) to e), the lower polariton states are more photonic (more negatively detuned). The dashed black and gray colors represent the energies for the exciton and cavity mode, while the red and blue colors represent the energies for the lower and upper polariton branches, respectively.

We measure angle-resolved reflectance spectra of the fabricated microcavities to observe the strong coupling behavior. A top DBR with 6.5 pairs of SiO_2/SiC is used to obtain a clear signal from the lower polaritons. Despite using a single spin-coating speed, the wavelength of the lower polariton slightly varies depending on the location of the top DBR flake. We speculate that this is due to the local variation in SMILES thickness, caused by the pressure applied during the transfer of top DBR onto the SMILES layer. We measure the reflectance at several locations of top DBR flakes, demonstrate that polaritons with varying detuning can be fabricated. Figure 2 presents microcavities with different detuning ordered from left to right. The figures on the right correspond to cavities with higher photonic fractions (more negatively detuned). We estimated the Rabi splitting value and detuning using a coupled oscillator model by fitting the measured lower polariton mode and energy of the R3B-SMILES exciton at 2.19 eV. The results of the fitting represent the lower and upper polariton branches as red and blue dots, respectively, and the cavity mode and the R3B-SMILES exciton as gray and black dots, respectively, in Figure 2. The individual detuning and Rabi splitting values for Figure 2 are provided in the Supplementary Material. The average measured Rabi splitting value is approximately 110 meV.

2.2. PL spectroscopy

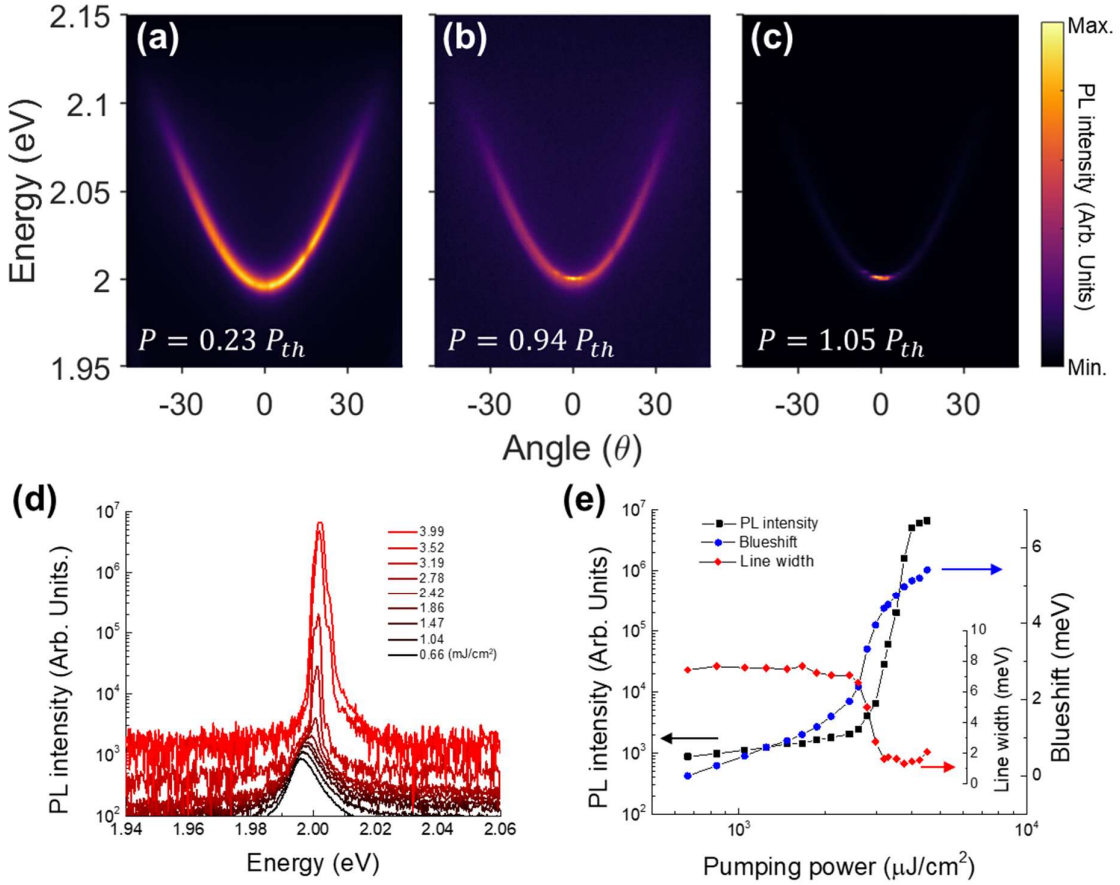

Figure 3. Angle-resolved PL spectrum and polariton condensation. a-c) Angle-resolved PL spectra for varying pump powers corresponding to 0.23 P_{th}, 0.94 P_{th},1.05 P_{th}, respectively. The threshold power P_{th} is 2.7 mJ/cm². With increasing pumping power, polaritons condense to the ground state. d) PL spectrum of polaritons at θ = 0° for different pumping powers. e) Pump power dependence of PL peak intensity (black squares), the blueshift (blue circles), and linewidth (red diamonds) of the lower polaritons.

We measure the angle-resolved PL spectrum with increasing pumping power to observe lower polaritons and polariton condensation. We use a fs-pulsed laser with a wavelength of 514 nm (~ 2.4 eV) to excite the sample non-resonantly. The pump beam has a broad Gaussian profile with a beam diameter of approximately 30 μm to exclude potential gradients and to avoid degradation at small pumping spot due to the heating or burning by the tightly focused laser.[27] Figures 3a-c show the angle-resolved PL spectrum under different pump power regimes. Below the condensation threshold, PL spectrum exhibits a broad energy-momentum distribution of the lower polariton branch, as shown in Figure 3a. With increasing pumping power, the polaritons condense into the ground state at θ = 0°, as shown in Figure 3b. Above the threshold density, most polaritons occupy the ground state, as shown in Figure 3c. The threshold pumping power

for condensation is 2.7 mJ/cm². In Figure 3d, we extract the spectrum at θ = 0°, the ground state, from the measured angle-resolved PL spectrum and plot it as a function of pump power. As the pump power increases, a sharp peak appears above the threshold. In Figure 3e, we present the pump power dependency of the PL peak intensity (black squares), the blueshift (blue circles), and the linewidth (red diamonds) of lower polaritons. Below the threshold density, the PL intensity exhibits a sublinear increase, which is commonly observed in organic materials due to PL quenching effects such as exciton-exciton annihilation.[4,22] However, above the threshold density, the PL intensity shows a nonlinear increase. The blueshift of the PL peak is also observed with increasing polariton density. The blueshift is due to the quenching of the Rabi splitting by saturation of molecular optical transitions and the Kerr-type nonlinearities in the organic polaritons.[13, 29] And above the threshold, as the polaritons condense into a single ground state, the coherence of the polaritons increases while dephasing processes are suppressed, resulting in the linewidth narrowing.[1]

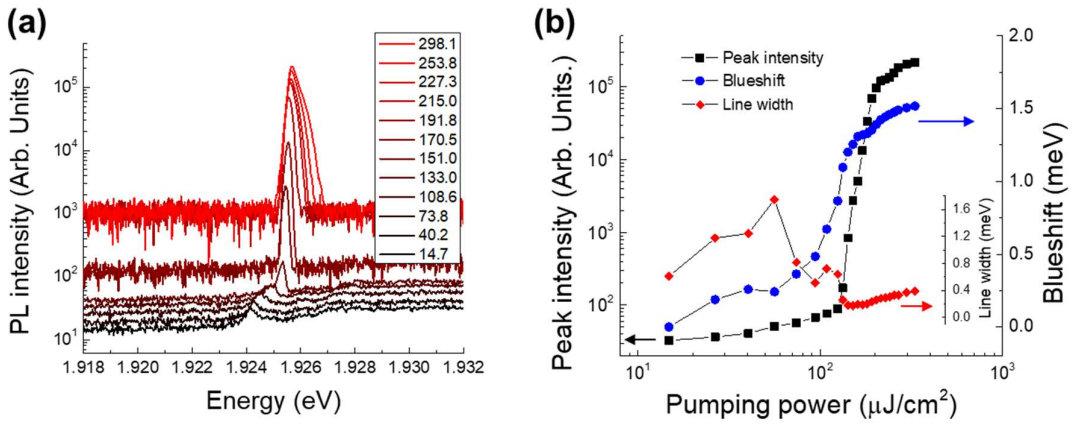

Figure 4. PL spectrum of polariton condensates having the narrowest linewidth. a) Selected PL spectra as a function of the pump power. b) Pump power dependence of peak intensity (black squares), peak energy (blue circles), and linewidth (red diamonds). The narrowest measured linewidth of the polariton condensates near the threshold is 175 μeV (0.058 nm).

We also fabricated microcavities with 8.5 pairs of SiO_2/SiC for the top DBR and measured the PL spectrum at different pump powers as shown in Figure 4a. Using more DBR pairs results in a cavity with a higher Q-factor. This microcavity is highly negatively detuned, with a photonic fraction of 95% for the lower polaritons. Figure 4b shows the pump power dependence of PL intensity, blueshift, and linewidth of the lower polaritons. We observe the linewidth of the lower polariton to be ~ 0.60 meV below the threshold from which we can estimate the Q-factor of the

microcavity by $Q = E_{LP}/(\Delta E_{LP}/|C|^2) \sim 3{,}000$ with the photonic fraction $|C|^2 = 0.95$.[30] Similar to Figure 3, the higher Q device shows the typical behavior of polariton condensation as pump power increases, but with a lower threshold of 133 μJ/cm². This threshold value is ~ 0.93 nJ/pulse, which is comparable to that of previous reports of molecular polariton condensates obtained in highly confined zero-dimensional geometry.[13] Owing to the larger negative detuning, this device shows only 1meV blue shift at threshold. Above the threshold, we obtain ultra-narrow linewidth emission corresponding to 175 μeV (0.058 nm) limited by the resolution of the spectrometer setup (123 μeV = 0.042 nm). Although a narrower linewidth of 0.02 nm has been reported in organic vertical cavity surface-emitting laser operating in the weak coupling regime[31], in the context of polariton lasing, our result is one of the narrowest reported which has implications in the coherence properties. (See Table.2 in the Supporting materials).

2.3. Coherence properties with Michelson interferometer

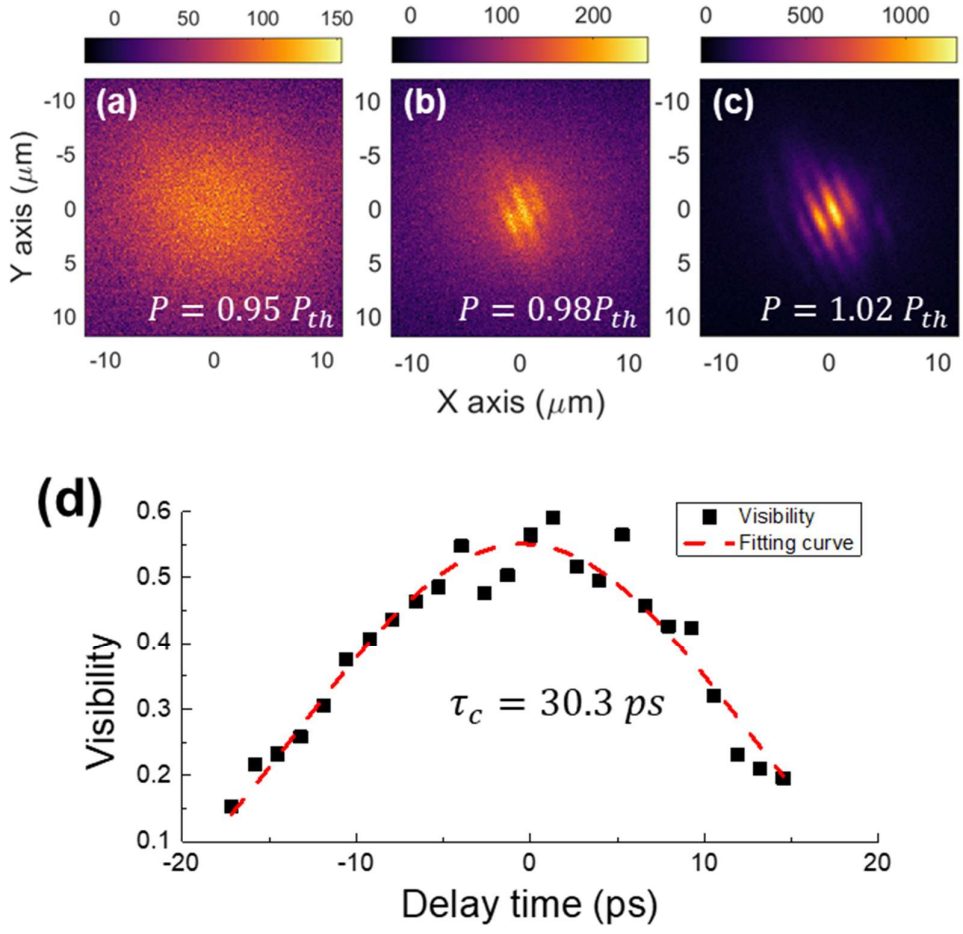

Figure 5. Coherence properties of polaritons. a-c) Interference maps of polaritons in real space as a function of pump power. Below the threshold (P = 0.95 P_{th}), polaritons show a uniform

intensity distribution without fringes. Above the threshold, polaritons form coherent condensates, and an interference fringe pattern is visible (P = 1.02 P_{th}). d) Temporal coherence of polariton condensates. The visibility of the fringe is plotted as a function of the delay time of two arms of the Michelson interferometer. The measured data are shown in black squares, and the fitting curve is shown in red dashed lines. The fitted coherence time is 30.3 ± 8.0 ps

One of the features of polariton condensation is the spontaneous formation of long-range spatial coherence, which can be measured by observing the interference pattern using a Michelson interferometer and retroreflector. In addition, temporal coherence can be measured by controlling the delay between the arms of the interferometer. The build-up of interference over a large area as the condensates provides evidence for the emergence of long-range order. Figures 5a-c show the interference map of polaritons for varying pump power. Below the threshold power, the interference map exhibits a broad distribution in real space without any interference (Figure 5a). However, at the threshold power, a weak interference fringe begins to appear at the center (Figure 5b). And above the threshold power, the polariton condensates shows clear interference fringes over a large area (Figure 5c), indicating the build-up of coherence in polariton condensates.

In addition to spatial coherence, the temporal coherence of the condensates can also be measured using the same interferometer configuration by varying the optical path length of the two arms with respect to each other. We define the fringe visibility of the interference pattern as $V = (I_{max} - I_{min})/(I_{max} + I_{min})$, where I_{max} and I_{min} are the intensity maximum and minimum of the interference. Figure 5d shows the extracted visibility as a function of delay between the two arms. The visibility decreases as the delay time moves away from the zero delay. The measured data is fitted with a Gaussian distribution, and the extracted temporal coherence is approximately 30.3 ± 8.0 ps. This value is an order of magnitude greater than previously reported results for organic material-based polaritons in planar microcavities.[11,28,32] Although longer temporal coherence of ~ 150 ps has been reported[13], it was observed in zero-dimensional cavities where the confinement enhances the coherence properties. (See Table.3 in the Supporting materials for comparison). From the temporal coherence measurement, we estimate the linewidth to be ~ 0.014 nm which is approximately four times smaller than the measured linewidth (0.058 nm) from the polariton lasing emission spectrum. This discrepancy is due to the resolution limit of our set up (0.042 nm).

3. Conclusion

We successfully observe strong light-matter interaction and room-temperature polariton condensation in all-DBR microcavities using SMILES. This is achieved through the DBR transfer method, which enables a higher Q-factor compared to the TP polaritons in the metal/DBR microcavities. In particular, we achieve polariton condensates with ultra-narrow linewidth of 175 μeV in an organic material-based planar microcavity in the strong coupling regime. Furthermore, through interferometry, we demonstrate the emergence of long-range phase coherence in the polariton condensed state with a temporal coherence of ~ 30.3 ± 8.0 ps, an order of magnitude higher than the previously reported values.[13,33,34] Although we have not measured our polariton condensate lifetimes, we assume that it would be on the same order as previously reported values of organic polaritons, i.e., on the order of a few picoseconds.[4] Notably, the temporal coherence of our organic polaritons exceeds the polariton lifetime, a phenomenon that has been previously reported.[13,33,34] For polaritons with Wannier-Mott excitons at low temperatures, the coherence time is affected by polariton-polariton interaction and polariton-reservoir interaction.[33,34] However, polaritons with Frenkel excitons cannot be explained in the same manner. Understanding their behavior requires a fundamental investigation into interparticle interaction as well as the decoherence mechanism of the Frenkel exciton-polaritons.

Recent studies have endeavored to understand the coherence properties of organic polaritons[35,36], but the underlying mechanisms for their unexpectedly long coherence times exceeding 10 ps remain unclear. One report hint at possible connection between population transfer and dark states as decoherence mechanisms.[36] However, further theoretical work is essential to for a comprehensive understanding of the coherence properties of molecular condensates. Furthermore, a recent experimental report has revealed that organic polaritons can achieve a high degree of second-order coherence at room temperature.[37] This result suggests that, despite their nonequilibrium and disordered nature, organic polariton condensates can maintain relatively low-intensity noise. Given the recent interest in room-temperature polaritons, our work highlights the significant potential of organic polaritons as coherent light sources operating at room temperature. Our results of narrow spectral linewidth and high temporal coherence in organic polariton systems represent a significant step toward room-temperature polariton-based device applications.

4. Methods

Sample fabrications: To synthesize R3B-SMILES, we mix the R3B dye as the perchlorate (ClO4–) salt and cyanostar (Halophore) and dissolves it in PMMA C2 solution (2% w/w PMMA in chlorobenzene, Kayaku Chem). The solution undergoes 48 hours of stirring at room temperature, synthesizing R3B-SMILES assemblies in the PMMA solution. The R3B-SMILES solution was then spin-coated on the SiO_2/TiO2 bottom DBR. We use plasma-enhanced chemical vapor deposition to deposit the SiO_2/SiC DBR for the top DBR onto a mica substrate. We take the SiO_2/SiC DBRs from the mica substrate with PDMS and transfer the peeled DBRs to spin-coated SMILES. And we take PDMS off from the SMILES. A portion of the SiO2/SiC DBRs remain in the SMILES and form microcavities.

Optical measurement and interferometry: Angle-resolved reflectance measurements were conducted with a broadband tungsten halogen lamp. The reflected signal was collected using an objective lens (0.8 NA). The signal was measured with a spectrometer (Princeton Instruments) and charged-coupled device camera (Princeton Instruments). PL spectrum measurements were conducted with a fs-pulsed laser (Light Conversion), which has 515 nm wavelength and 10 kHz repetition rate. A 550 nm long pass filter was used to eliminate laser signal in PL measurement. Interference fringes were measured with a Michelson interferometer and a retroreflector. Visibility is extracted by identifying the maximum intensity I_{max} and minimum intensity I_{min} values within the interference fringes and calculating the $V = (I_{max} - I_{min})/(I_{max} + I_{min})$. One arm of the interferometer was placed on a computer-controlled stage (Thorlabs). We measured the temporal coherence by moving the mirror with the stage. The visibility values measured as a function of delay time were fitted using a Gaussian function to extract the coherence time.

Supporting Information

Supporting Information is available from the Wiley Online Library or from the author.

Acknowledgements

The authors were supported by the U.S. Air Force Office of Scientific Research − MURI Grant FA9550-22-1-0317 (VMM and RKY), NSF - OMA-2328993 (DC), and NSF DMR-2019444 - IMOD STC (SZ). The authors acknowledge the use of the nanofabrication and imaging facility at ASRC, CUNY.

Received: ((will be filled in by the editorial staff))
Revised: ((will be filled in by the editorial staff))
Published online: ((will be filled in by the editorial staff))

References

[1] J. Kasprzak, M. Richard, S. Kundermann, A. Baas, P. Jeambrun, J. M. J. Keeling, F. M. Marchetti, M. H. Szymańska, R. André, J. L. Staehli, V. Savona, P. B. Littlewood, B. Deveaud, L. S. Dang, Nature 2006, 443, 409.

[2] H. Deng, G. Weihs, D. Snoke, J. Bloch, Y. Yamamoto, Proc. Natl. Acad. Sci. 2003, 100, 15318.

[3] S. Kim, B. Zhang, Z. Wang, J. Fischer, S. Brodbeck, M. Kamp, C. Schneider, S. Höfling, H. Deng, Phys. Rev. X 2016, 6, 011026.

[4] S. Kéna-Cohen, S. R. Forrest, Nat. Photonics 2010, 4, 371.

[5] R. Su, C. Diederichs, J. Wang, T. C. H. Liew, J. Zhao, S. Liu, W. Xu, Z. Chen, Q. Xiong, Nano Lett. 2017, 17, 3982.

[6] J. Zhao, R. Su, A. Fieramosca, W. Zhao, W. Du, X. Liu, C. Diederichs, D. Sanvitto, T. C. H. Liew, Q. Xiong, Nano Lett. 2021, 21, 3331.

[7] S. Chénais, S. Forget, Polym. Int. 2012, 61, 390.

[8] J. Keeling, S. Kéna-Cohen, Annu. Rev. Phys. Chem. 2020, 71, 435.

[9] S. Kéna-Cohen, M. Davanço, S. R. Forrest, Phys. Rev. Lett. 2008, 101, 116401.

[10] S. Kéna-Cohen, S. A. Maier, D. D. C. Bradley, Adv. Opt. Mater. 2013, 1, 827.

[11] J. D. Plumhof, T. Stöferle, L. Mai, U. Scherf, R. F. Mahrt, Nat. Mater. 2014, 13, 247.

[12] C. P. Dietrich, A. Steude, L. Tropf, M. Schubert, N. M. Kronenberg, K. Ostermann, S. Höfling, M. C. Gather, Sci. Adv. 2016, 2, e1600666.

[13] S. Betzold, M. Dusel, O. Kyriienko, C. P. Dietrich, S. Klembt, J. Ohmer, U. Fischer, I. A. Shelykh, C. Schneider, S. Höfling, ACS Photonics 2020, 7, 384.

[14] R. T. Grant, P. Michetti, A. J. Musser, P. Gregoire, T. Virgili, E. Vella, M. Cavazzini, K. Georgiou, F. Galeotti, C. Clark, J. Clark, C. Silva, D. G. Lidzey, Adv. Opt. Mater. 2016, 4, 1615.

[15] A. V. Zasedatelev, A. V. Baranikov, D. Sannikov, D. Urbonas, F. Scafirimuto, V. Yu. Shishkov, E. S. Andrianov, Y. E. Lozovik, U. Scherf, T. Stöferle, R. F. Mahrt, P. G. Lagoudakis, Nature 2021, 597, 493.

[16] D. A. Sannikov, A. V. Baranikov, A. D. Putintsev, M. Misko, A. V. Zasedatelev, U. Scherf, P. G. Lagoudakis, Nat. Commun. 2024, 15, 5362.

[17] A. V. Zasedatelev, A. V. Baranikov, D. Urbonas, F. Scafirimuto, U. Scherf, T. Stöferle, R. F. Mahrt, P. G. Lagoudakis, Nat. Photonics 2019, 13, 378.

[18] R. K. Yadav, S. Satapathy, P. Deshmukh, B. Datta, A. Sharma, A. H. Olsson, J. Chen, B. W. Laursen, A. H. Flood, M. Y. Sfeir, V. M. Menon, Nano Lett. 2024, acs.nanolett.4c00586.

[19] M. Dusel, S. Betzold, O. A. Egorov, S. Klembt, J. Ohmer, U. Fischer, S. Höfling, C. Schneider, Nat. Commun. 2020, 11, 2863.

[20] J. Witt, A. Mischok, F. Tenopala Carmona, S. Hillebrandt, J. F. Butscher, M. C. Gather, ACS Photonics 2024, 11, 1844.

[21] C. R. Benson, L. Kacenauskaite, K. L. VanDenburgh, W. Zhao, B. Qiao, T. Sadhukhan, M. Pink, J. Chen, S. Borgi, C.-H. Chen, B. J. Davis, Y. C. Simon, K. Raghavachari, B. W. Laursen, A. H. Flood, Chem 2020, 6, 1978.

[22] P. Deshmukh, S. Satapathy, E. Michail, A. H. Olsson, R. Bushati, R. K. Yadav, M. Khatoniar, J. Chen, G. John, B. W. Laursen, A. H. Flood, M. Y. Sfeir, V. M. Menon, ACS Photonics 2024, 11, 348.

[23] A. Ge, L. Sun, M. Xie, H. Cui, D. Zhou, L. Ma, X. Zhang, Y. Huan, H. Tian, W. Jing, B. Yao, S. Wang, X. Shen, W. Lu, Adv. Opt. Mater. 2024, 12, 2303286.

[24] E. Y. Paik, L. Zhang, S. Hou, H. Zhao, Y. Chou, S. R. Forrest, H. Deng, Adv. Opt. Mater. 2023, 11, 2201440.

[25] E. A. Amargianitakis, S. A. Kazazis, G. Doundoulakis, G. Stavrinidis, G. Konstantinidis, E. Delamadeleine, E. Monroy, N. T. Pelekanos, Microelectron. Eng. 2020, 228, 111276.

[26] C. Rupprecht, N. Lundt, M. Wurdack, P. Stepanov, E. Estrecho, M. Richard, E. A. Ostrovskaya, S. Höfling, C. Schneider, Appl. Phys. Lett. 2021, 118, 103103.

[27] M. Wouters, I. Carusotto, C. Ciuti, Phys. Rev. B 2008, 77, 115340.

[28] F. Scafirimuto, D. Urbonas, U. Scherf, R. F. Mahrt, T. Stöferle, ACS Photonics 2018, 5, 85.

[29] T. Yagafarov, D. Sannikov, A. Zasedatelev, K. Georgiou, A. Baranikov, O. Kyriienko, I. Shelykh, L. Gai, Z. Shen, D. Lidzey, P. Lagoudakis, Commun. Phys 2020, 3, 18.

[30] P. Tsotsis, P. S. Eldridge, T. Gao, S. I. Tsintzos, Z. Hatzopoulos, P. G. Savvidis, New J. Phys. 2012, 14, 023060.

[31] V. Bulović, V. G. Kozlov, V. B. Khalfin, S. R. Forrest, Science 1998, 279, 553.

[32] K. S. Daskalakis, S. A. Maier, S. Kéna-Cohen, Phys. Rev. Lett. 2015, 115, 035301.

[33] A. P. D. Love, D. N. Krizhanovskii, D. M. Whittaker, R. Bouchekioua, D. Sanvitto, S. Al Rizeiqi, R. Bradley, M. S. Skolnick, P. R. Eastham, R. Andre´, Le Si Dang. Phys. Rev. Lett. 2008, 101, 067404.

[34] A. Askitopoulos, L. Pickup, S. Alyatkin, A. Zasedatelev, K.G. Lagoudakis, W. Langbein, P.G. Lagoudakis. *Arxiv*, 1911.08981, Submitted: November, 2019.

[35] W. Hu, I. Gustin, T. D. Krauss, I. Franco, J. Phys. Chem. Lett. 2022, 13 (49), 11503-11511.

[36] B. X. K. Chng, W. Ying, Y. Lai, A. N. Vamivakas, S. T. Cundiff, T. D. Krauss, P. Huo, J. Phys. Chem. Lett. 2024, 15, XXX, 11773–11783

[37] A. D. Putintsev, A. V. Zasedatelev, V. Y. Shishkov, M. Misko, D. A. Sannikov, E. S. Andrianov, Y. E. Lozovik, U. Scherf, P. G. Lagoudakis. Phys. Rev. B. 2024, 110, 045125.

Supporting Information

Highly coherent room-temperature molecular polariton condensates

*Daegwang Choi, Serena Zachariah, Ravindra Kumar Yadav, and Vinod. M. Menon**

Table 1. Detuning and Hopefield coefficients from reflectance measurements

Sample	Cavity mode energy [eV]	Rabi splitting [eV]	Detuning [eV]	Photonic fraction $\lvert C^2 \rvert$	Lower polariton energy [eV]
1	2.123	0.107	0.067	0.765	2.097
2	2.095	0.110	0.095	0.826	2.070
3	2.069	0.114	0.121	0.863	2.046
4	2.048	0.110	0.142	0.895	2.030
5	2.018	0.112	0.172	0.918	2.000

Table 2. Organic material-based microcavity works

Reference	Active materials	Q-factor	Strong coupling	Wavelength of lower polariton [nm]	Linewidth of polariton emission after lasing [nm]	Linewidth of polariton emission after lasing [meV]	Threshold pump power
[1]	BP1T-CN	~ 350	X	499	~ 0.2	~ 1.0	45 μJ/cm^2
[2]	BODIPY-G1	~ 600	O	568	~ 0.1	~ 0.38	6 mJ/cm^2
[3]	BSBCz:CBP	2,230	X	460	0.24	~ 1.40	1.7 μJ/cm^2
[4]	mCherry	7,500	O	641	~ 0.059 [a), b)]	~ 0.18 [a), b)]	0.78 nJ/pulse
[5]	BODIPY-Br	~ 540	O	569	~ 0.42	~ 1.6	295 μJ/cm^2
[6]	2L-F/4L-F, LiF	302	O	430	~ 0.12	0.8	12 μJ/cm^2
[7]	BSFCz	517	O	464	~ 0.07	0.4	9.7 μJ/cm^2
[8]	R3B-SMILES	150	O	590	~ 2.0	7.1	0.2 mJ/cm^2
[9]	Alq_3:DCM	-	X	618	0.02 ± 0.01	0.064	320 μJ/cm^2
This work	R3B-SMILES	3,000	O	644	0.058	0.175	133 μJ/cm^2

[a)] Confined state; [b)] Measurement resolution limit

Table 3. Temporal coherence of organic polaritons

Reference	Active materials	Coherence time [ps]	Linewidth of polariton emission after lasing [meV]
[10]	MeLPPP	~ 2	~ 2
[11]	TDAF	0.81	1
[12]	MeLPPP	~ 1	1.5 [a)]
[4]	mCherry	150 [a)]	0.18 [a), b)]
This work	R3B-SMILES	30.3	0.175

[a)] Confined state; [b)] Measurement resolution limit

References

[1] Y. Tanaka, K. Goto, K. Yamashita, T. Yamao, S. Hotta, F. Sasaki, H. Yanagi, *App. Phys. Lett.* 2015, 107, 163303.

[2] D. Sannikov, T. Yagafarov, K. Georgiou, A. Zasedatelev, A. Baranikov, L. Gai, Z. Shen, D. Lidzey, P. Lagoudakis, *Adv. Opt. Mater.* 2019, 7, 17, 1900163.

[3] Y. Hu, F. Bencheikh, S. Chénais, S. Forget, X. Liu, C. Adachi, *Appl. Phys. Lett*. 2020, 117, 153301.

[4] S. Betzold, M. Dusel, O. Kyriienko, C. P. Dietrich, S. Klembt, J. Ohmer, U. Fischer, I. A. Shelykh, C. Schneider, S. Höfling, *ACS Photonics* 2019, 7, 2, 384–392.

[5] K. E. McGhee, A. Putintsev, R. Jayaprakash, K. Georgiou, M. E. O'Kane, R. C. Kilbride, E. J. Cassella, M. Cavazzini, D. A. Sannikov, P. G. Lagoudakis, D. G. Lidzey, *Sci. Rep*. 2021, 11, 20879.

[6] M. Wei, M. Fang, S. K. Rajendran, W.-Y. Lai, G. A Turnbull, I. D. Samuel, *Adv. Photonics Res.* 2020, 2, 1, 2000044.

[7] M. Wei, A. Ruseckas, V. T. Mai, A. Shukla, I. Allison, S.-C. Lo, E. B Namdas, G. A Turnbull, I. D. Samuel, *Laser Photonics Rev.* 2021, 15, 8, 2100028.

[8] P. Deshmukh, S. Satapathy, E. Michail, A. H. Olsson, R. Bushati, R. K. Yadav, M. Khatoniar, J. Chen, G. John, B. W. Laursen, A. H. Flood, M. Y. Sfeir, V. M. Menon, ACS Photonics 2024, 11, 2, 348-355.

[9] V. Bulović, V. G. Kozlov, V. B. Khalfin, S. R. Forrest, Science 1998, 279, 553.

[10] J. D. Plumhof, T. Stöferle, L. Mai, U. Scherf, R. F. Mahrt. *Nat. Mater.* 2014, 13, 247–252

[11] K. S. Daskalakis, S. A. Maier, S. Kéna-Cohen, Phys. Rev. Lett. 2015, 115, 035301.

[12] F. Scafirimuto, D. Urbonas, U. Scherf, R. F. Mahrt, T. Stöferle, ACS Photonics 2018, 5, 85.